Reprinted from June 1986, Vol. 108, Journal of Applied Mechanics

Combined Loading of a Fully Plastic Ligament Ahead of an Edge-Crack

C. F. Shih
Division of Engineering,
Brown University,
Providence, R.I. 02912

J. W. Hutchinson
Division of Applied Sciences,
Harvard University,
Cambridge, Mass. 02138

Complete, accurate numerical results are given for the solution to the problem of a semi-infinite crack aligned perpendicularly to the free-edge of a semi-infinite half space in which the ligament is subject to arbitrary combinations of bending and tension or compression. The material is an incompressible, pure power-law deformation theory solid. Conditions of plane strain are assumed. Approximate solutions are proposed for predominantly bending loadings and also for predominantly stretching loadings.

1 Introduction

Accurate numerical results will be presented for the basic problem of a semi-infinite crack approaching the free edge of a semi-infinite plane, as depicted in Fig. 1. The remote stresses acting on the upper-half plane are equivalent to a net load per unit thickness P and a net moment per unit thickness M taken about the origin in the sense shown. This is a Mode I problem, and attention is directed to the plane strain problem with $\epsilon_{33} = \epsilon_{13} = \epsilon_{23} = 0$. The study is carried out within the context of small strain theory, and the material of the cracked body is taken to be described by J_2 deformation theory for an incompressible pure power-law stress-strain behavior. In uniaxial tension the material deforms according to

$$\epsilon/\epsilon_o = (\sigma/\sigma_o)^n \tag{1.1}$$

where σ_o and ϵ_o are the reference stress and strain. Under multi-axial stress states, σ_{ij}, the strain is

$$\epsilon_{ij}/\epsilon_o = \frac{3}{2}(\sigma_e/\sigma_o)^{n-1} s_{ij}/\sigma_o \tag{1.2}$$

Here, s_{ij} is the stress deviator and $\sigma_e = (3s_{ij}s_{ij}/2)^{1/2}$ is the effective stress. (In earlier papers on pure power-law problems we have introduced an additional convenient scale factor α multiplying the right hand sides of (1.1) and (1.2). In this paper α has been absorbed into ϵ_o).

Approximate solutions to semi-infinite crack problems have been used to model the effect of deep part-through cracks in plates subject to combined tension and bending. In particular, such solutions play a central role in the development of the line-spring model for analyzing the effect of surface cracks in pressure vessel walls (Rice, 1972, and Parks and White, 1982).

This paper begins with the derivation of some fairly general relationships for arbitrary small strain deformation theory materials and then proceeds to specialize them to the power-law material. Numerical results are presented for quantities of interest over the full range of combined loading. The effect of shifting the origin about which the moment is defined is also discussed, and approximate analytical solutions are proposed.

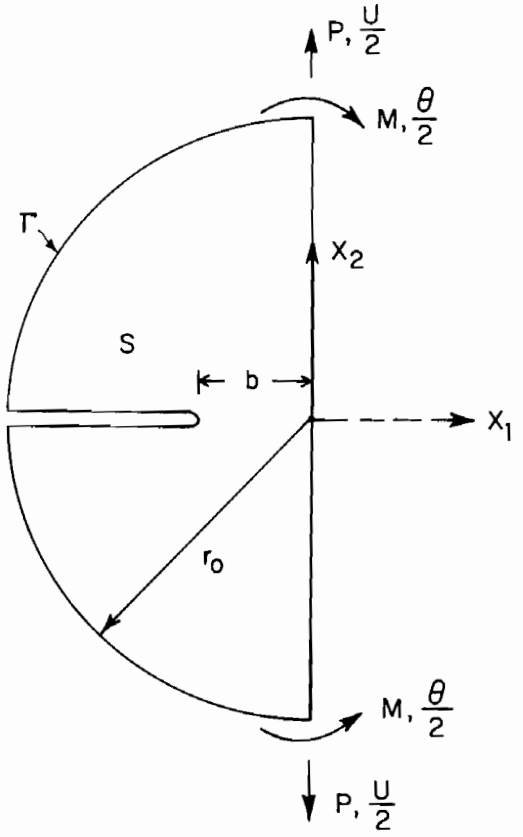

Fig. 1 Conventions

Contributed by the Applied Mechanics Division for presntation at the Winter Annual Meeting, Anaheim, CA, December 7–12, 1986, of the American Society of Mechanical Engineers.

Discussion on this paper should be addressed to the Editorial Department, ASME, United Engineering Center, 345 East 47th Street, New York, N.Y. 10017, and will be accepted until two months after final publication of the paper itself in the JOURNAL OF APPLIED MECHANICS. Manuscript received by ASME Applied Mechanics Division, April 23, 1985. Paper No. 86-WA/APM-1.

2 Some General Relationships for Finite and Infinite Geometries

At this stage, consider a body characterized by a general deformation theory in which $w(\epsilon)$ is the strain energy density and $\phi(\sigma)$ is the complementary stress energy density so that

$$\sigma_{ij}=\frac{\partial w}{\partial \epsilon_{ij}},\quad \epsilon_{ij}=\frac{\partial \phi}{\partial \sigma_{ij}} \text{ and } \sigma_{ij}\epsilon_{ij}=\phi+w \tag{2.1}$$

Consider a body occupying a finite region S, such as that in Fig. 1, and let Γ denote the portion of the body of S in the upper-half plane other than the traction-free crack faces and the traction-free edge along $x_1=0$. Prescribe in-plane displacements on Γ

$$u_\alpha=\frac{U}{2}\delta_{\alpha 2}+\frac{\Theta}{2}e_{\alpha\beta}x_\beta \tag{2.2}$$

where the sense of Θ is shown in Fig. 1 and $\delta_{\alpha\beta}$ is the Kronecker delta and $e_{\alpha\beta}$ is the permutation symbol. Opposite-signed prescriptions are made in the lower-half plane.

The force-like variables P and M are identified most directly through the external virtual work expression as

$$2\int_\Gamma T_\alpha \delta u_\alpha ds=\left(\int_\Gamma T_2 ds\right)\delta U + \left(\int_\Gamma e_{\alpha\beta}x_\beta T_\alpha ds\right)\delta\Theta \equiv P\delta U+M\delta\Theta \tag{2.3}$$

where $T_\alpha=\sigma_{\alpha\beta}n_\beta$ is the traction vector. In both (2.2) and (2.3) the origin of the coordinates (x_1, x_2) is taken at the free edge as shown in Fig. 1. Other choices are possible and may be preferred for certain purposes. The effect of shifting the origin of the coordinates is discussed in Section 5.

By (2.1) and the principle of virtual work,

$$PdU+Md\Theta=\int_S \sigma_{\alpha\beta}d\epsilon_{\alpha\beta}dS=\int_S dwdS \tag{2.4}$$

Thus, with the overall strain energy defined as

$$W(U,\Theta)=\int_S wdS \tag{2.5}$$

it follows that

$$P=\frac{\partial W}{\partial U} \text{ and } M=\frac{\partial W}{\partial \Theta} \tag{2.6}$$

The complementary connections may be derived similarly as

$$U=\frac{\partial \Phi}{\partial P} \text{ and } \Theta=\frac{\partial \Phi}{\partial M} \tag{2.7}$$

where

$$\Phi(P,M)=\int_S \Phi dS \tag{2.8}$$

In addition,

$$PU+M\Theta=W+\Phi \tag{2.9}$$

Now imagine that the stress-strain behavior of the material is such that W and Φ are well defined in the limit as the outer contour Γ is expanded to infinity (e.g., $r_o\to\infty$ in Fig. 1). For the power-law material (1.2) this limit is well defined as long as $n>1$. However, a linear material ($n=1$) is excluded from consideration unless $P=0$. By dimensional considerations similar to those first exploited by Rice et al. (1973), it necessarily follows that the functional dependence of W for the semi-infinite crack problem on the uncracked ligament, b, U and Θ is of the form

$$W=b^2F(U/b,\Theta) \tag{2.10}$$

where F depends implicitly on material properties.

The energy release rate, J, for the semi-infinite body is

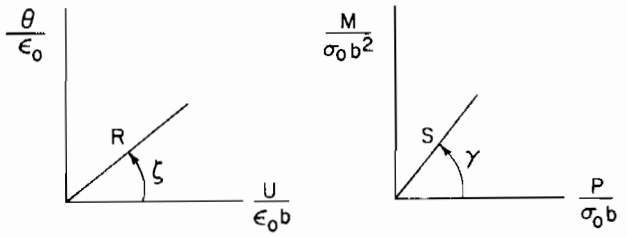

Fig. 2 Nondimensional displacement and load variables

$$J=\frac{dW}{db}=2bF-U\frac{\partial F}{\partial(U/b)}=\frac{2W}{b}-\frac{PU}{b} \tag{2.11}$$

where $P=b\partial F/\partial(U/b)$ from (2.6), and (2.10) has been used.

It has become fairly common practice (Turner, 1980) to write the relationship between J and W under combined bending and tension loadings as

$$J=\eta W/b \tag{2.12}$$

so that, from (2.11), the "eta factor" is given precisely by

$$\eta=2-PU/W \tag{2.13}$$

For either P or U vanishing, $\eta=2$. As an approximation, η has been taken to be 2 for load combinations typical of several "bend-type" geometries, but this approximation is of dubious accuracy in general. For example, when either $M=0$ or $\Theta=0$ one finds using (2.9) that

$$\eta=1-\Phi/W \tag{2.14}$$

which is necessarily less than unity since Φ and W are each inherently positive. For a pure-power-law material this becomes $\eta=(n-1)/n$.

3 Relations Among J, P, M and Θ for Semi-infinite Crack in a Power-Law Material

Because the equilibrium equations and the strain-displacement equations are linear, the dimensional forms for W and Φ from the solution for the pure power-law material (1.2) are

$$W=\sigma_o\epsilon_o b^2 f_W[U/(\epsilon_o b),\Theta/\epsilon_o] \tag{3.1}$$

$$\Phi=\sigma_o\epsilon_o b^2 f_\phi[P/(\sigma_o b),\ M/(\sigma_o b^2)] \tag{3.2}$$

where f_W and f_ϕ are dimensionless functions of the arguments indicated. Moreover, it also follows from the linearity of the equilibrium and strain-displacement equations and the character of the stress-strain law (1.2) that f_W and f_ϕ satisfy

$$f_W[-U/(\epsilon_o b),-\Theta/\epsilon_o]=f_W[U/(\epsilon_o b),\Theta/\epsilon_o] \tag{3.3}$$

$$f_\phi[-P/(\sigma_o b),-M/(\sigma_o b^2)]=f_\phi[P/(\sigma_o b),M/(\sigma_o b^2)] \tag{3.4}$$

Of course, contact between the crack faces is disregarded in writing these relations. Our interest is restricted to the range of variables such that the crack faces are not in contact; nevertheless, for mathematical purposes it is useful to produce the solution over the full range of the variables under the ficitious assumption that the crack faces may overlap.

From the equations listed in the previous section it is seen that knowledge of either f_W for f_ϕ fully determines the relationships among J, P, M, U and Θ. There are various ways to present the numerical results for f_W or f_ϕ, but the pure power character of the stress-strain law favors the following approach. Let

$$R=\left[\left(\frac{U}{\epsilon_o b}\right)^2+\left(\frac{\Theta}{\epsilon_o}\right)^2\right]^{1/2} \text{ and } \zeta=\arctan\left[\frac{\Theta/\epsilon_o}{U/(\epsilon_o b)}\right] \tag{3.5}$$

be polar coordinates in the plane of $U/\epsilon_o b$ and Θ/ϵ_o as in-

Table 1 Normalized functions for $n = 3$

ζ	γ	η	f	f'	g	k	h	h'
0.0	31.1	0.667	0.693	0.557	0.462	1.079	1.71E-01	-4.12E-01
5.0	31.6	0.735	0.739	0.492	0.543	1.101	1.68E-01	-3.35E-01
10.0	31.9	0.799	0.778	0.418	0.622	1.119	1.66E-01	-2.67E-01
15.0	32.4	0.861	0.811	0.340	0.698	1.134	1.64E-01	-2.05E-01
20.0	32.9	0.921	0.837	0.255	0.771	1.145	1.62E-01	-1.48E-01
25.0	33.3	0.980	0.856	0.167	0.838	1.153	1.61E-01	-9.45E-02
30.0	33.9	1.040	0.867	0.080	0.901	1.158	1.61E-01	-4.43E-02
35.0	34.5	1.100	0.870	-0.010	0.956	1.160	1.60E-01	5.71E-03
40.0	35.0	1.160	0.865	-0.100	1.003	1.157	1.61E-01	5.60E-02
45.0	35.5	1.222	0.852	-0.190	1.041	1.152	1.61E-01	1.08E-01
50.0	36.1	1.286	0.832	-0.275	1.070	1.143	1.63E-01	1.61E-01
55.0	36.7	1.354	0.804	-0.355	1.089	1.130	1.65E-01	2.18E-01
60.0	37.3	1.425	0.770	-0.429	1.097	1.113	1.67E-01	2.80E-01
65.0	37.9	1.501	0.729	-0.497	1.095	1.092	1.71E-01	3.49E-01
70.0	38.6	1.582	0.683	-0.556	1.081	1.068	1.75E-01	4.28E-01
75.0	39.3	1.671	0.633	-0.606	1.057	1.038	1.81E-01	5.21E-01
80.0	40.1	1.769	0.578	-0.644	1.023	1.004	1.90E-01	6.33E-01
85.0	41.1	1.878	0.521	-0.669	0.978	0.964	2.01E-01	7.75E-01
90.0	42.2	2.000	0.462	-0.679	0.924	0.916	2.18E-01	9.62E-01
95.0	43.6	2.135	0.403	-0.673	0.860	0.861	2.44E-01	1.22E+00
100.0	45.3	2.282	0.345	-0.649	0.787	0.795	2.87E-01	1.62E+00
105.0	47.8	2.429	0.290	-0.601	0.705	0.715	3.70E-01	2.30E+00
110.0	51.5	2.544	0.241	-0.524	0.612	0.615	5.62E-01	3.67E+00
115.0	58.2	2.541	0.200	-0.406	0.508	0.486	1.19E+00	7.29E+00
116.0	60.3	2.514	0.193	-0.377	0.485	0.456	1.48E+00	8.69E+00
117.0	62.7	2.474	0.187	-0.346	0.462	0.426	1.89E+00	1.05E+01
118.0	65.6	2.423	0.181	-0.313	0.438	0.395	2.48E+00	1.29E+01
119.0	69.1	2.357	0.176	-0.278	0.414	0.363	3.36E+00	1.59E+01
120.0	73.4	2.277	0.171	-0.241	0.390	0.332	4.69E+00	1.98E+01
121.0	78.6	2.184	0.167	-0.204	0.365	0.302	6.69E+00	2.44E+01
122.0	84.7	2.083	0.164	-0.167	0.342	0.275	9.53E+00	2.91E+01
122.8	90.0	2.000	0.162	-0.139	0.324	0.257	1.24E+01	3.15E+01
123.0	91.8	1.974	0.161	-0.131	0.319	0.252	1.34E+01	3.25E+01
124.0	100.0	1.858	0.160	-0.095	0.296	0.233	1.81E+01	3.22E+01
125.0	109.4	1.736	0.158	-0.059	0.275	0.219	2.29E+01	2.56E+01
126.0	120.0	1.606	0.157	-0.022	0.253	0.211	2.64E+01	1.11E+01
127.0	131.9	1.462	0.157	0.018	0.230	0.211	2.66E+01	-9.14E+00
128.0	144.2	1.307	0.158	0.061	0.207	0.220	2.27E+01	-2.63E+01
129.0	155.8	1.143	0.160	0.107	0.182	0.238	1.65E+01	-3.33E+01
130.0	166.0	0.972	0.162	0.157	0.157	0.267	1.06E+01	-3.09E+01
131.0	174.3	0.804	0.165	0.207	0.133	0.302	6.58E+00	-2.48E+01
132.0	180.7	0.648	0.169	0.257	0.110	0.342	4.13E+00	-1.88E+01
133.0	185.7	0.505	0.174	0.305	0.088	0.383	2.69E+00	-1.41E+01
134.0	189.8	0.377	0.180	0.352	0.068	0.426	1.82E+00	-1.07E+01
135.0	193.1	0.264	0.186	0.399	0.049	0.470	1.28E+00	-8.19E+00
140.0	201.7	0.000	0.229	0.567	0.000	0.644	4.44E-01	-3.29E+00
145.0	205.0	0.018	0.283	0.655	0.005	0.756	2.89E-01	-2.01E+00
150.0	206.8	0.118	0.342	0.698	0.040	0.834	2.36E-01	-1.44E+00
155.0	207.9	0.230	0.404	0.711	0.093	0.892	2.12E-01	-1.12E+00
160.0	208.8	0.333	0.466	0.710	0.155	0.943	1.96E-01	-8.97E-01
165.0	209.5	0.429	0.527	0.690	0.226	0.985	1.87E-01	-7.33E-01
170.0	210.1	0.515	0.586	0.658	0.302	1.021	1.80E-01	-6.04E-01
175.0	210.6	0.594	0.642	0.613	0.381	1.052	1.74E-01	-5.00E-01
180.0	211.1	0.667	0.693	0.557	0.462	1.079	1.71E-01	-4.12E-01

Table 2 Normalized functions for $n = 5$

ζ	γ	η	f	f'	g	k	h	h'
0.0	30.2	0.800	0.911	0.636	0.729	1.265	4.46E-02	-1.56E-01
5.0	30.5	0.859	0.963	0.551	0.827	1.280	4.38E-02	-1.25E-01
10.0	30.8	0.914	1.007	0.460	0.921	1.293	4.31E-02	-9.86E-02
15.0	31.2	0.968	1.043	0.363	1.009	1.303	4.26E-02	-7.43E-02
20.0	31.6	1.019	1.070	0.263	1.091	1.311	4.22E-02	-5.19E-02
25.0	32.0	1.071	1.089	0.160	1.166	1.316	4.19E-02	-3.09E-02
30.0	32.5	1.123	1.098	0.057	1.233	1.319	4.17E-02	-1.09E-02
35.0	33.0	1.175	1.099	-0.045	1.291	1.319	4.17E-02	8.60E-03
40.0	33.6	1.229	1.090	-0.147	1.340	1.316	4.19E-02	2.82E-02
45.0	34.1	1.284	1.073	-0.248	1.378	1.311	4.22E-02	4.88E-02
50.0	34.6	1.341	1.047	-0.346	1.404	1.303	4.28E-02	7.07E-02
55.0	35.1	1.402	1.013	-0.439	1.419	1.292	4.35E-02	9.43E-02
60.0	35.8	1.466	0.971	-0.524	1.423	1.277	4.47E-02	1.21E-01
65.0	36.4	1.536	0.921	-0.602	1.415	1.259	4.63E-02	1.51E-01
70.0	37.1	1.611	0.866	-0.671	1.394	1.237	4.84E-02	1.87E-01
75.0	37.9	1.692	0.805	-0.731	1.362	1.211	5.10E-02	2.32E-01
80.0	38.7	1.783	0.739	-0.780	1.317	1.180	5.46E-02	2.88E-01
85.0	39.6	1.885	0.669	-0.815	1.261	1.144	5.97E-02	3.64E-01
90.0	40.7	2.000	0.597	-0.834	1.194	1.099	6.77E-02	4.73E-01
95.0	41.9	2.130	0.524	-0.838	1.116	1.048	7.91E-02	6.33E-01
100.0	44.0	2.269	0.452	-0.805	1.024	0.970	1.08E-01	9.64E-01
105.0	45.9	2.420	0.383	-0.768	0.928	0.895	1.49E-01	1.49E+00
110.0	48.9	2.557	0.319	-0.691	0.815	0.790	2.62E-01	2.84E+00
115.0	55.9	2.552	0.265	-0.531	0.677	0.619	9.45E-01	9.45E+00
116.0	57.9	2.528	0.256	-0.494	0.648	0.582	1.32E+00	1.28E+01
117.0	60.3	2.491	0.248	-0.453	0.618	0.542	1.96E+00	1.79E+01
118.0	63.3	2.438	0.240	-0.408	0.586	0.499	3.10E+00	2.63E+01
119.0	67.0	2.369	0.234	-0.359	0.554	0.455	5.24E+00	4.02E+01
120.0	71.8	2.281	0.228	-0.306	0.520	0.410	9.53E+00	6.40E+01
121.0	77.8	2.180	0.223	-0.252	0.486	0.368	1.81E+01	1.02E+02
122.0	85.0	2.070	0.219	-0.199	0.454	0.330	3.42E+01	1.55E+02
122.6	90.0	2.000	0.217	-0.167	0.434	0.309	4.95E+01	1.79E+02
123.0	93.6	1.953	0.216	-0.146	0.422	0.298	6.20E+01	2.10E+02
124.0	103.7	1.831	0.214	-0.095	0.392	0.274	1.01E+02	2.25E+02
125.0	115.0	1.704	0.213	-0.045	0.363	0.259	1.40E+02	1.48E+02
126.0	127.6	1.569	0.213	0.007	0.334	0.255	1.54E+02	-2.60E+01
127.0	141.0	1.421	0.213	0.064	0.303	0.264	1.27E+02	-1.90E+02
128.0	153.9	1.262	0.215	0.125	0.271	0.287	7.76E+01	-2.26E+02
129.0	165.2	1.095	0.218	0.191	0.238	0.324	3.79E+01	-1.67E+02
130.0	174.6	0.922	0.221	0.262	0.204	0.373	1.64E+01	-9.70E+01
131.0	182.0	0.750	0.227	0.336	0.170	0.432	6.97E+00	-5.16E+01
132.0	187.7	0.587	0.233	0.411	0.137	0.497	3.09E+00	-2.72E+01
133.0	192.3	0.434	0.241	0.487	0.105	0.567	1.46E+00	-1.47E+01
134.0	196.0	0.293	0.250	0.565	0.073	0.640	7.29E-01	-8.24E+00
135.0	199.1	0.165	0.261	0.644	0.043	0.716	3.87E-01	-4.78E+00
140.0	205.3	0.010	0.329	0.859	0.003	0.946	9.20E-02	-1.20E+00
145.0	206.5	0.158	0.406	0.895	0.064	1.019	7.25E-02	-8.01E-01
150.0	207.5	0.285	0.485	0.913	0.138	1.082	6.04E-02	-5.68E-01
155.0	208.1	0.401	0.564	0.903	0.226	1.128	5.47E-02	-4.38E-01
160.0	208.6	0.502	0.642	0.875	0.322	1.165	5.12E-02	-3.49E-01
165.0	209.1	0.590	0.716	0.832	0.422	1.196	4.88E-02	-2.84E-01
170.0	209.5	0.667	0.787	0.779	0.525	1.224	4.68E-02	-2.32E-01
175.0	209.9	0.737	0.852	0.712	0.627	1.246	4.56E-02	-1.91E-01
180.0	210.2	0.800	0.911	0.636	0.729	1.264	4.46E-02	-1.56E-01

dicated in Fig. 2. Because f_W is homogeneous of degree $N+1$ in $U/\epsilon_o b$ and Θ/ϵ_o, one can further specialize (3.1) to

$$W = \sigma_o \epsilon_o b^2 R^{N+1} f(\zeta, N) \tag{3.6}$$

where f is a dimensionless function of $N \equiv 1/n$ and ζ which by (3.3) has the periodicity

$$f(\zeta + \pi, N) = f(\zeta, N) \tag{3.7}$$

Thus, knowledge of $f(\zeta, N)$ completely determines the relations among all variables of interest. In particular, from (2.6)

$$P = \sigma_o b R^N [(N+1) f \cos\zeta - f' \sin\zeta] \tag{3.8}$$

$$M = \sigma_o b^2 R^N [(N+1) f \sin\zeta + f' \cos\zeta] \tag{3.9}$$

where $f' = \partial f(\zeta, N)/\partial\zeta$. From (2.11) it follows that

$$J = \sigma_o \epsilon_o b R^{N+1} \{[2 - (N+1)\cos^2\zeta] f + f' \sin\zeta\cos\zeta] \tag{3.10}$$

$$\equiv \sigma_o \epsilon_o b R^{N+1} g(\zeta, N) \tag{3.11}$$

and then, from (2.13), that

$$\eta(\zeta, N) = g/f = 2 - (N+1)\cos^2\zeta + (f'/f)\sin\zeta\cos\zeta \tag{3.12}$$

Alternatively, if P and M are preferred as independent variables, let

$$S = \left[\left(\frac{P}{\sigma_o b}\right)^2 + \left(\frac{M}{\sigma_o b^2}\right)\right]^{1/2} \text{ and } \gamma = \arctan\left[\frac{M/(\sigma_o b^2)}{P/(\sigma_o b)}\right] \tag{3.13}$$

Now, since f_ϕ is homogeneous of degree $n+1$ in P and M,

$$\Phi = \sigma_o \epsilon_o b^2 S^{n+1} h(\gamma, n) \tag{3.14}$$

where $h(\gamma + \pi, n) = h(\gamma, n)$. From (2.7),

$$U = \epsilon_o b S^n [(n+1) h \cos\gamma - h' \sin\gamma] \tag{3.15}$$

$$\Theta = \epsilon_o S^n [(n+1) h \sin\gamma + h' \cos\gamma] \tag{3.16}$$

where $h' = \partial h(\gamma, n)/\partial\gamma$.

The relations between the polar load variables and the polar displacement variables follow directly from (3.8) and (3.9) as

$$S = R^N [(N+1)^2 f^2 + (f')^2]^{1/2} \equiv k(\zeta, N) R^N \tag{3.17}$$

and

$$\gamma = \arctan\left\{\frac{(N+1) f \sin\zeta + f' \cos\zeta}{(N+1) f \cos\zeta - f' \sin\zeta}\right\} \tag{3.18}$$

Finally, from the fact that $\Phi = NW$, it follows that

$$h = N f k^{-(N+1)/N} \tag{3.19}$$

and

$$J = \sigma_o \epsilon_o b (S/k)^{n+1} g \tag{3.20}$$

4 Numerical Results

As has already been emphasized, all information regarding the relationships among M, Θ, P, U and J is contained in the function $f(\zeta, N)$. This function has been computed numerically using a finite element method specially designed for incompressible materials as has been described in prior publications (Shih and Needleman, 1984a, 1984b). Details peculiar to the present problem are discussed in the Appendix. In addition, a number of consistency checks on the numerical solution are also discussed in the Appendix. These checks give some indication of the accuracy of the computed quantities.

The numerical data is presented in Tables 1–3. Values of f, f', g, h, h', η, γ and k are given at 5 deg intervals of ζ for $n = 3$, 5, and 10. Within the range of ζ from 115 deg to 135 deg, γ changes rapidly so values are given for each 1 deg interval of ζ within this range. This range spans pure bending (i.e., $P = 0$, $\gamma = 90$ deg), and data for $\gamma = 90$ deg is also included in

Table 3 Normalized functions for $n = 10$

ζ	γ	η	f	f'	g	k	h	h'
0.0	29.5	0.900	1.072	0.667	0.965	1.355	3.79E-03	-2.36E-02
5.0	29.8	0.952	1.126	0.571	1.073	1.364	3.70E-03	-1.87E-02
10.0	30.1	1.002	1.172	0.471	1.174	1.372	3.61E-03	-1.45E-02
15.0	30.4	1.049	1.208	0.366	1.268	1.378	3.54E-03	-1.07E-02
20.0	30.8	1.096	1.236	0.258	1.354	1.383	3.48E-03	-7.27E-03
25.0	31.2	1.142	1.253	0.150	1.431	1.387	3.44E-03	-4.10E-03
30.0	31.7	1.189	1.262	0.041	1.500	1.388	3.41E-03	-1.11E-03
35.0	32.3	1.237	1.261	-0.066	1.559	1.388	3.42E-03	1.80E-03
40.0	32.8	1.287	1.250	-0.173	1.608	1.386	3.45E-03	4.77E-03
45.0	33.4	1.337	1.230	-0.278	1.645	1.382	3.51E-03	7.94E-03
50.0	33.9	1.389	1.202	-0.382	1.669	1.376	3.60E-03	1.14E-02
55.0	34.5	1.445	1.164	-0.479	1.682	1.367	3.74E-03	1.54E-02
60.0	35.1	1.504	1.118	-0.570	1.682	1.356	3.93E-03	2.01E-02
65.0	35.8	1.568	1.065	-0.655	1.669	1.342	4.19E-03	2.58E-02
70.0	36.5	1.637	1.004	-0.731	1.644	1.325	4.55E-03	3.32E-02
75.0	37.2	1.713	0.937	-0.799	1.606	1.304	5.04E-03	4.30E-02
80.0	38.0	1.798	0.865	-0.856	1.555	1.280	5.73E-03	5.67E-02
85.0	38.8	1.892	0.788	-0.903	1.491	1.252	6.65E-03	7.62E-02
90.0	40.1	2.000	0.708	-0.924	1.416	1.208	8.84E-03	1.15E-01
95.0	41.1	2.123	0.627	-0.945	1.331	1.170	1.12E-02	1.68E-01
100.0	42.3	2.264	0.544	-0.944	1.231	1.118	1.60E-02	2.77E-01
105.0	44.6	2.410	0.463	-0.896	1.117	1.031	3.31E-02	6.39E-01
110.0	47.7	2.564	0.388	-0.813	0.988	0.919	9.88E-02	2.07E+00
115.0	53.6	2.575	0.324	-0.652	0.834	0.743	8.46E-01	1.70E+01
116.0	55.5	2.555	0.313	-0.609	0.799	0.699	1.60E+00	3.12E+01
117.0	57.8	2.520	0.303	-0.559	0.762	0.650	3.44E+00	6.36E+01
118.0	60.7	2.468	0.293	-0.503	0.724	0.597	8.51E+00	1.46E+02
119.0	64.5	2.396	0.285	-0.440	0.683	0.541	2.48E+01	3.82E+02
120.0	69.4	2.305	0.278	-0.372	0.641	0.482	8.61E+01	1.15E+03
121.0	75.9	2.196	0.272	-0.301	0.597	0.424	3.40E+02	3.76E+03
122.0	84.1	2.076	0.267	-0.229	0.555	0.373	1.38E+03	1.18E+04
122.6	90.0	2.000	0.265	-0.187	0.531	0.346	3.08E+03	2.17E+04
123.0	94.5	1.947	0.264	-0.158	0.514	0.331	5.12E+03	3.06E+04
124.0	107.3	1.809	0.262	-0.086	0.474	0.301	1.44E+04	4.73E+04
125.0	122.0	1.665	0.261	-0.015	0.435	0.288	2.35E+04	1.34E+04
126.0	137.5	1.514	0.261	0.059	0.396	0.293	1.88E+04	-4.21E+04
127.0	152.2	1.353	0.263	0.136	0.356	0.320	7.36E+03	-3.80E+04
128.0	164.6	1.187	0.266	0.217	0.316	0.365	1.75E+03	-1.43E+04
129.0	174.5	1.017	0.271	0.303	0.275	0.425	3.34E+02	-3.73E+03
130.0	182.2	0.848	0.277	0.392	0.235	0.497	6.11E+01	-8.66E+02
131.0	188.1	0.684	0.284	0.484	0.194	0.577	1.22E+01	-2.07E+02
132.0	192.8	0.530	0.294	0.577	0.156	0.661	2.77E+00	-5.45E+01
133.0	196.5	0.390	0.305	0.671	0.119	0.750	7.21E-01	-1.59E+01
134.0	199.5	0.263	0.317	0.766	0.083	0.842	2.12E-01	-5.11E+00
135.0	202.1	0.150	0.331	0.862	0.050	0.936	6.89E-02	-1.79E+00
140.0	206.8	0.092	0.420	1.076	0.039	1.171	7.40E-03	-1.90E-01
145.0	207.0	0.290	0.512	1.060	0.148	1.201	6.84E-03	-1.41E-01
150.0	207.7	0.421	0.605	1.053	0.255	1.246	5.38E-03	-9.36E-02
155.0	208.1	0.536	0.695	1.017	0.373	1.273	4.90E-03	-7.17E-02
160.0	208.5	0.630	0.782	0.971	0.493	1.298	4.46E-03	-5.53E-02
165.0	208.6	0.711	0.864	0.907	0.615	1.314	4.28E-03	-4.49E-02
170.0	208.9	0.781	0.940	0.835	0.735	1.330	4.09E-03	-3.64E-02
175.0	209.3	0.843	1.010	0.757	0.852	1.344	3.90E-03	-2.92E-02
180.0	209.5	0.900	1.072	0.667	0.965	1.355	3.80E-03	-2.36E-02

the Tables. Use of the data can be illustrated by two special cases.

Pure Stretching ($\Theta = 0$). Pure stretching is defined with $\Theta = 0$ and $U > 0$ so that $\zeta = 0$ deg and $R = U/(\epsilon_o b)$. Then

$$J = \sigma_o \epsilon_o b (U/\epsilon_o b)^{N+1} g(0, N) \tag{4.1}$$

where $g(0, 1/3) = 0.462$, $g(0, 1/5) = 0.729$, and $g(0, 1/10) = 0.965$. The corresponding values of P and M can be obtained from (3.8) and (3.9). Note that $\gamma \simeq 30$ deg in pure stretching, and, from (2.14), $\eta = 1 - N$.

Pure Bending. In pure bending, $P = 0$ and $M > 0$ so that $\gamma = 90$ deg and $S = M/(\sigma_o b^2)$. By (3.20)

$$J = \sigma_o \epsilon_o b \left(\frac{M}{k \sigma_o b^2} \right)^{n+1} g \tag{4.2}$$

The values of k and g associated with $\gamma = 90$ deg are included in the Tables, as are h and h', which allow one to determine U and Θ from (3.15) and (3.16). Equation (4.2) can be rewritten in the form given by Shih and Needleman (1984a) as

$$J = \sigma_o \epsilon_o b h_1(n) (M/M_o)^{n+1} \tag{4.3}$$

where, for all n, the reference moment is

$$M_o = \mu_2 \sigma_o b^2 \quad (\mu_2 = 0.364) \tag{4.4}$$

The results from Shih and Needleman (1984a) for a deeply-cracked strip with a ligament to width ratio of 1/8 are $h_1(3) = 1.30$, $h_1(5) = 1.16$ and $h_1(10) = 0.97$. The corresponding results converted from (4.2) using the values in the Tables are $h_1(3) = 1.31$, $h_1(5) = 1.15$ and $h_1(10) = 0.92$. In pure bending $\eta = 2$.

The overall strain energy W is equal to the work of the combined loads through their respective displacement quantities. If the loads are increased so that M and P maintain a fixed proportion, the deformation theory W is also exactly equal to

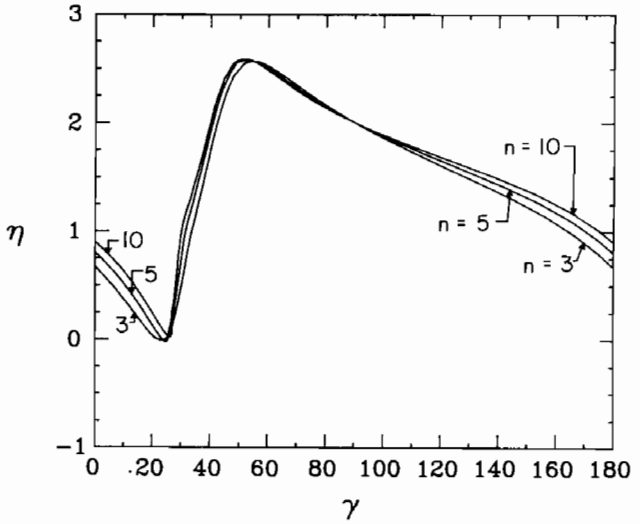

Fig. 3(a) The eta-factor as a function of γ

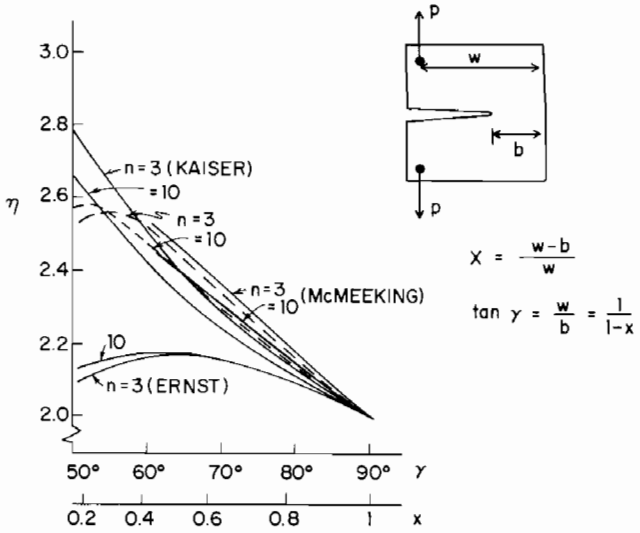

Fig. 3(b) The eta-factor as a function of γ for the range appropriate to a compact specimen

the work done on the body if the material is described by a pure-power flow theory (i.e., an incremental plasticity theory). The significance of the "eta factor," η, defined in (2.12) is that it permits the determination of J directly from the work done on a specimen by the applied loads. Curves of the eta factor are presented in Figs. 3*a* and 3*b*. In Fig. 3*a*, η is plotted as a function of γ for $n = 3$, 5 and 10 over the full range of loadings. The same variation of η is shown in Fig. 3*b* for $n = 3$ and 10 for γ between 50 deg and 90 deg, corresponding to the range of γ appropriate to standard compact tension specimens. Predictions from the present calculations are shown as dashed line curves in Fig. 3*b*. Predictions for η from other investigators are also shown and will be discussed below. To apply the deeply-cracked solution to a compact tension specimen, we let $M = Pw$ where w is the distance between the line of action of the load P and the back face of the specimen. Thus, $\tan \gamma = w/b$. The parameter $x = (w - b)/w$ is frequently used to characterize the geometry of the compact tension specimen. It is related to γ by $\tan \gamma = 1/(1 - x)$, and the variation of η with x is also included in Fig. 3*b*.

A typical value of x for a compact tension specimen is 1/2 corresponding to $\gamma = 63.4$ with $\eta = 2.46$ for $n = 3$ and $\eta = 2.42$ for $n = 10$, according to the present calculations. These values are substantially above the pure bending value, $\eta = 2$. Several investigators have developed approximations for η to account

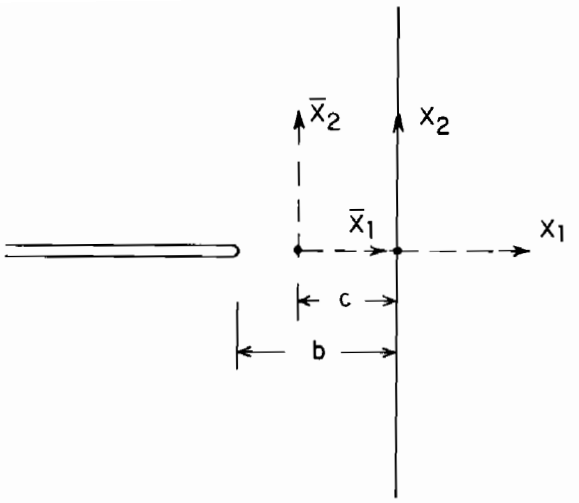

Fig. 4 Conventions for shift of origin

for combined loading effects present in the compact tension specimen, including Ernst (1983), Kaiser (1985), and McMeeking (1984). In each case, the approximation for the plastic part of J leads to an expression of the form

$$J=\eta_1 b^{-1}\int_0^{\Delta} P d\Delta+\eta_2 b^{-1}\int_0^{P}\Delta dP \tag{4.5}$$

where η_1 and η_2 depend on x or γ (but not on n) and Δ denotes the plastic part of the overall load-point displacement. For the pure power law material, this expression reduces to

$$J=(\eta_1+\eta_{2/n})b^{-1}W\equiv\eta b^{-1}W \tag{4.6}$$

We have used the variations of η_1 and η_2 with x given by Ernst (1983), Kaiser (1985), and McMeeking (1984) to plot the curves of η in Fig. 3*b* for the pure power material. Ernst's results for η are about 13 percent below the present predictions for $x=1/2$. McMeeking's results are exceedingly close to those obtained here over the range $0.4\le x\le 1$ for which he tabulates his η_1 and η_2. This suggests that the more general formula (4.5), which is not tied to the power law material, may be used with confidence with McMeeking's values of η_1 and η_2. Kaiser's predictions for η are also in reasonable accord with those obtained over this same range. However, outside this range his predictions deviate substantially from the present ones, as is already evident in Fig. 3*b*. We also note that Ernst's results become significantly in error in the vicinity of $\gamma=26$ deg, which is his "pure tension" limit. Ernst's notion of a pure tension limit is tied to the approximate form of the stress distribution he assumes. His approximation in this limit assumes the stress is uniform across the ligament so that P acts through the mid-point of the ligament. Unlike the special states of pure stretching and pure bending which are defined precisely, the "pure tension" state does not appear to have a precise meaning outside the context of his approximation.

5 Shift of Origin

For some applications another choice of origin may be preferred, and two other particular choices will be illustrated. Consider a second set of coordinates $(\bar{x}_1, \bar{x}_2)$ with $\bar{x}_2=x_2$ and $\bar{x}_1=x_1+c$, as shown in Fig. 4. The quantities P and Θ are invariant with respect to this coordinate shift, but denote the moment about the new origin $(\bar{x}_1=0, \bar{x}_2=0)$ by $\bar{M}$ where from moment equilibrium

$$\bar{M}=M-cP \tag{5.1}$$

The remote displacements are rewritten as

$$u_\alpha=\frac{\bar{U}}{2}\delta_{\alpha 2}+\frac{\Theta}{2}e_{\alpha\beta}\bar{x}_\beta \tag{5.2}$$

where, by comparison with (2.2), it is readily established that

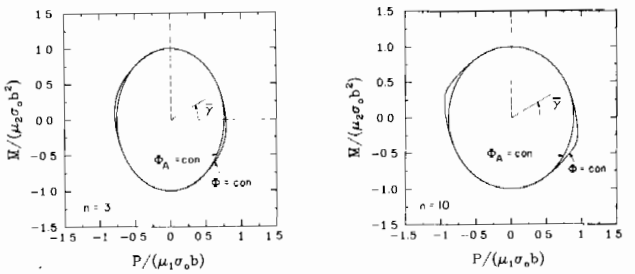

Fig. 5 Contours of constant Φ for choice of origin at the axis of rotation for pure bending as specified by equation (5.8)

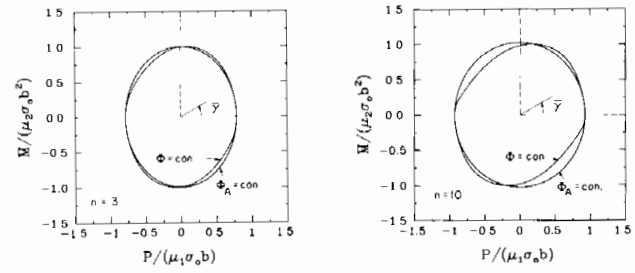

Fig. 6 Contours of constant Φ for choice of origin such that $\bar{M}=0$ when $\Theta=0$ according to equation (5.9)

$$\bar{U}=U+c\Theta \tag{5.3}$$

In deriving the relations of Sections 2 and 3 we could have equally well used the variable pairs $(\bar{U}, \Theta)$ and $(P, \bar{M})$ associated with $c\neq 0$. With the exception of the expressions for J, the formulas connecting the variables remain unchanged. However, given the fact that results have been presented for the choice $c=0$, it is probably simplest to use these results together with (5.1) and (5.3) to shift to a set of coordinates with $c\neq 0$. The alternative is to form a new table of functions (f, f', etc.) for the new choice from the functions presented for $c=0$.

The form of formula (2.11) for J is not preserved under a shift of origin. By (5.3), (2.11) becomes

$$J=\frac{2W}{b}-\frac{P(\bar{U}-c\Theta)}{b} \tag{5.4}$$

and (2.13) is

$$\eta=2-P(\bar{U}-c\Theta)/W \tag{5.5}$$

To determine numerical results for J in terms of shifted variables, $(P, \bar{M})$ or $(\bar{U}, \Theta)$, it is probably easiest to use the relations (5.1) and (5.3) to transform to (P, M) or (U, Θ) and then use Tables 1-3.

Origin at the "Axis of Rotation" for Pure Bending. As an illustration, choose c such that $\bar{U}=0$ when $P=0$. That is, the origin is located such that in pure bending the remote displacements in the upper-half plane are given by

$$u_\alpha=\frac{\Theta}{2}e_{\alpha\beta}\bar{x}_\beta \tag{5.6}$$

By (5.3) and (3.5), $\bar{U}=0$ requires

$$\frac{c}{b}=-\frac{U}{\Theta b}=-\frac{1}{\tan\zeta} \tag{5.7}$$

where the value of ζ is that associated with $\gamma=90$ deg (i.e., $P=0$). From Table 1, we obtain

$$c/b=\begin{cases}0.644 & (n=3)\\ 0.640 & (n=5)\\ 0.639 & (n=10)\end{cases} \tag{5.8}$$

The slip-line field for the perfectly-plastic material from the analysis of Green and Hundy (1956) gives $c/b=0.631$. This choice of origin will be considered again in the next section in

connection with an approximation for predominantly bending behavior.

Choice of Origin such that $\bar{M}=0$ in Pure Stretching. As a second illustration, choose c such that $\bar{M}=0$ when $\Theta=0$. That is, choose the origin so that the moment about this origin vanishes under pure stretching. By (5.1), this gives $c/b=M/(bP)$ for $\zeta=0$ deg. From (3.8) and (3.9), one obtains

$$\frac{c}{b}=\frac{f'(0)}{(N+1)f(0)}=\begin{cases}0.603 & (n=3)\\ 0.582 & (n=5)\\ 0.566 & (n=10)\end{cases} \tag{5.9}$$

This choice will be used in developing an approximation for predominantly stretching behavior.

6 Two Approximations

Predominantly Bending States. Take the origin at the axis of rotation for pure bending as specified by (5.7) and (5.8). With $\bar{M}$ measured about this choice of origin, contours of constant ϕ are shown in Fig. 5 for $n=3$ and $n=10$. For the power-law material these contours are self-similar, and the particular contour shown was chosen such that the vertical intercept is unity. The nondimensional load variables used in the plot are

$$\frac{P}{\mu_1\sigma_o b} \text{ and } \frac{\bar{M}}{\mu_2\sigma_o b^2} \tag{6.1}$$

Here, $\mu_2=0.364$ so that $\mu_2\sigma_o b^2$ is the Green-Hundy (1956) limit load for the perfectly-plastic problem in pure bending. We take $\mu_1=2/\sqrt{3}$ so that $\mu_1\sigma_o b$ would be the limit load in pure stretching, if the stress state for this perfectly-plastic problem were plane strain tension across the entire ligament. It is not certain that this is the correct limiting state; nevertheless, this choice for μ_1 is suitable for the normalization. The two contours in Fig. 5 were derived from the numerical results given in Tables 1 and 3. (The limit of these contours as $n\to\infty$ is the limiting yield surface under the combined loads.)

By virtue of the choice of origin such that $\bar{U}=\partial\Phi/\partial P=0$ when $P=0$, it follows that the contour of $\Phi=$ con. in Fig. 5 must intercept the vertical $\bar{M}$ axis with zero slope, as can be seen. We construct an approximation in the range of predominantly bending states (i.e., $|\bar{M}/(\mu_2\sigma_o b^2)|>|P/(\mu_1\sigma_o b)|$), by choosing an ellipse to approximate the contour of $\Phi=$ con. in such a way that the curvature, as well as the intercept and slope, matches that of the actual contour at the vertical intercept. The result can be seen in Fig. 5, and the specification of the approximation is as follows.

With Φ_A denoting the approximate ϕ, we take

$$\Phi_A=\frac{\epsilon_o\sigma_o b^2}{(n+1)}\left\{c_1(n)\left(\frac{P}{\mu_1\sigma_o b}\right)^2+c_2(n)\left(\frac{\bar{M}}{\mu_2\sigma_o b^2}\right)^2\right\}^{(n+1)/2} \tag{6.2}$$

This choice ensures that the approximating contour intercepts the $\bar{M}$ axis with zero slope; $c_2(n)$ is chosen so that $\Phi_A=\phi$ when $P=0$. We determined $c_1(n)$ by requiring that $\Phi_A=\phi$ at an angle $\bar{\gamma}$ about 30 from the horizontal axis in the first quadrant of the plane in Fig. 5. This simple procedure leads to a very small error in the curvature of the approximating contour at $P=0$ but slightly extends the range of the approximation so that it is accurate everywhere in the first quadrant except in the vicinity of $M=0$, as can be seen in Fig. 5. The values of c_1 and c_2 so determined are

$$\begin{aligned} c_1(3) &= 1.2141 \quad & c_2(3) &= 0.9329\\ c_1(5) &= 0.9663 \quad & c_2(5) &= 0.8838\\ c_1(10) &= 0.8433 \quad & c_2(10) &= 0.8828 \end{aligned} \tag{6.3}$$

and the corresponding locations of the origin to which $\bar{M}$ is referred are given by (5.8).

Let H^2 denote the quadratic terms within the brackets in (6.2), so that

$$\Phi_A=\sigma_o\epsilon_o b^2H^{n+1}/(n+1) \tag{6.4}$$

It follows then that the associated approximate displacement quantities are

$$\begin{aligned} \bar{U} &= \partial\Phi_A/\partial P=\epsilon_o bH^{n-1}(c_1/\mu_1)P/(\mu_1\sigma_o b)\\ \Theta &= \partial\Phi_A/\partial\bar{M}=\epsilon_o H^{n-1}(c_2/\mu_2)\bar{M}/(\mu_2\sigma_o b^2) \end{aligned} \tag{6.5}$$

Moreover, the associated approximate overall strain energy $W_A=n\Phi_A$ is readily found to be

$$W_A=\sigma_o\epsilon_o b^2nL^{(n+1)/n} \tag{6.6}$$

where

$$L^2=\frac{\mu_1^2}{c_1(n)}\left(\frac{\bar{U}}{\epsilon_o b}\right)^2+\frac{\mu_2^2}{c_2(n)}\left(\frac{\Theta}{\epsilon_o}\right)^2 \tag{6.7}$$

Using the connections $P=\partial W_A/\partial\bar{U}$ and $\bar{M}=\partial W_A/\partial\Theta$, one can derive the associated load variables in terms of U and Θ.

With these results in hand, the approximation for J follows immediately from (5.4) i.e.,

$$J_A=[2W_A-P(\bar{U}-c\Theta)]/b=[2n\Phi_A-P(\bar{U}-c\Theta)]/b \tag{6.8}$$

where $\bar{U}$ and Θ are obtained from (6.5) if P and $\bar{M}$ are prescribed or P and $\bar{M}$ are obtained from (6.6) if $\bar{U}$ and Θ are prescribed. We have compared J_A with the "actual" J given by the full numerical results over the full range of angle $\bar{\gamma}$ measured from the P axis in Fig. 5. For

$$30 \text{ deg}\le\bar{\gamma}\le 100 \text{ deg} \tag{6.9}$$

J_A differs from J by less than 1 percent for $n=3$ and by less than 3 percent for $n=10$. For the range

$$15 \text{ deg}\le\bar{\gamma}\le 125 \text{ deg} \tag{6.10}$$

J_A differs from J by no more than 6 percent for both $n=3$ and $n=10$. The approximation does become inaccurate in the vicinity of the P axis. With $\bar{M}=0$, the J_A differs from J by 16 percent for $n=3$ and 12 percent for $n=10$. Thus, this approximation is only recommended for use in the range (6.9) or possibly (6.10).

Predominantly Stretching States. Now take the origin as specified by (5.9) such that $\bar{M}=0$ when $\Theta=0$. Contours of $\Phi=$ con. with this choice of origin are shown in Fig. 6. The same nondimensional load variables (6.1) are used except, of course, now $\bar{M}$ is taken with respect to the new choice of origin. The same constant value of Φ as was used in Fig. 5 is used in plotting Fig. 6. Since $\Theta=\partial\Phi/\partial\bar{M}=0$ at the intercept with the P axis, the contour necessarily has an infinite slope there, as can be seen.

The approximation for predominantly stretching states (i.e., $|P/(\mu_1\sigma_o b)|>|\bar{M}/(\mu_2\sigma_o b^2)|$) is obtained in the same way as in the previous instance, except that now the ellipse is chosen so that it approximates the contour in the vicinity of the P axis. The functional form of the approximation is precisely that given above. All of equations (6.2) through (6.8) carry over, except that the coefficients c_1 and c_2 in (6.3) will be different. In this approximation, $c_1(n)$ is determined by requiring $\Phi_A=\Phi$ for $\bar{M}=0$ and $c_2(n)$ is chosen to provide a good approximation to the curvature at the intercept with the P axis. Here we chose $c_2(n)$ such that $\Phi_A=\Phi$ at $\bar{\gamma}\simeq 15$ deg, where now $\bar{\gamma}$ is defined as the angular measure from the P axis in Fig. 6. The resulting coefficients are

$$\begin{aligned} c_1(3) &= 1.1267 \quad & c_2(3) &= 0.9321\\ c_1(5) &= 0.8625 \quad & c_2(5) &= 0.8882\\ c_1(10) &= 0.7408 \quad & c_2(10) &= 0.8051 \end{aligned} \tag{6.11}$$

As is clear from the contours in Fig. 6, the range of validity of this approximation is not nearly as extensive as in the previous case. For

$$0 \text{ deg}\le\bar{\gamma}\le 15 \text{ deg} \tag{6.12}$$

the error in J_A, compared to our numerical results for J, does not exceed 4 percent when $n=3$ nor 6 percent when $n=10$. But

outside this range the approximation becomes increasingly inaccurate, and thus its use is only recommended for the range (6.12). Together, the two approximations, for predominantly bending states and predominantly stretching states, do span essentially the entire range of practical interest.

Acknowledgment

The work of J. W. Hutchinson was supported in part by the National Science Foundation under Grant MEA-82-13925 and by the Division of Applied Sciences, Harvard University. The work of C. F. Shih was supported by the Electric Power Research Institute through Grant RP1757-17-1 and the US Department of Energy through Grant DE-AC02-80-ER10556. The computations reported on here were carried out on a VAX-11/780 computer at the Brown University, Division of Engineering, Computational Mechanics Computer Facility. This facility was made possible by grants from the US National Science Foundation (Grant ENG78-19378), the General Electric Foundation and the Digital Equipment Corporation.

References

Ernst, H. A., 1983, "Unified Solution for J Ranging Continuously from Pure Bending to Pure Tension," in *ASTM STP 791*, American Society for Testing and Materials, pp. I-499–I-519.

Green, A. P., and Hundy, B. B., 1956, "Initial Plastic Yielding in Notch Bend Tests," *Journal of the Mechanics and Physics of Solids*, Vol. 4, pp. 128–144.

Kaiser, S., 1985, "The J-Integral and Tearing Modulus for a SEN Specimen under Bending and Tension," *Engineering Fracture Mechancis*, Vol. 22, pp. 737–749.

Li, F. Z., Shih, C. F., and Needleman, A., 1985, "A Comparison of Methods for Calculating Energy Release Rates," *Engineering Fracture Mechanics*, Vol. 21, pp. 405–421.

McMeeking, R. M., 1984, "Estimates of J-Integral for Elastic-Plastic Specimens in Large Scale Yielding," *ASME Journal of Engineering Materials and Technology*, Vol. 106, pp. 278–284.

Parks, D. M., and White, C. S., 1982, "Elastic-Plastic Line Spring Finite Element for Surface-Cracked Plates and Shells," *Journal of Pressure Vessel Technology*, Vol. 184, pp. 287–292.

Rice, J. R., 1972, "The Line Spring Model for Surface Flaws," in *The Surface Crack: Physical Problems and Computational Solutions*, Swedlow, ed., ASME, pp. 171–186.

Rice, J. R., Paris, P. C., and Merkle, J. G., 1973, "Some Further Results of J-Integral Analysis and Estimates," in *ASTM STP 536*, American Society for Testing and Materials, pp. 231–245.

Shih, C. F., and Needleman, A., 1984a, "Fully Plastic Crack Problems: Part I – Solutions by a Penalty Method," ASME JOURNAL OF APPLIED MECHANICS, Vol. 51, pp. 48–56.

Shih, C. F., and Needleman, A., 1984b, "Fully Plastic Crack Problems: Part II – Application of Consistency Checks," ASME JOURNAL OF APPLIED MECHANICS, Vol. 51, pp. 57–64.

Turner, C. E., 1980, "The Ubiquitous η Factor," in *ASTM STP 700*, American Society for Testing and Materials, pp. 314–337.

Young, D. M., and Gregory, R. T., 1972, *A Survey of Numerical Mathematics*, Vols. I and II, Addison-Wesley, Reading, Mass.

APPENDIX

Finite Element Analysis of Fully Plastic Crack Problems

Penalty Formulation, Element Choice and Mesh Design. The numerical solutions for the deeply cracked panel presented in Section 4 were obtained by a finite element reduced integration penalty method (Shih and Needleman, 1984a). Fully plastic solutions obtained by the method have been shown to satisfy rather stringent consistency relations (Shih and Needleman, 1984b). We employed the 9-noded Lagrangian element to model the geometry depicted in Fig. 1. The volumetric stiffness matrix is obtained by 2 by 2 (reduced) integration while the deviatoric stiffness matrix is obtained by 3 by 3 (regular) integration. Hydrostatic stresses are computed at the 2 by 2 Gauss points and deviatoric stresses at the 3 by 3 Gauss points. To obtain the total stress at the 3 by 3 Gauss points, we used Lagrangian bilinear shape functions in conjunction with the values of hydrostatic stress at the 2 by 2 Gauss points to determine the hydrostatic stress at the 3 by 3 Gauss points.

With reference to the geometry in Fig. 1 we modelled only the upper-half plane since the problem possesses reflective symmetry about the crack plane. We experimented with r_o/b ratios of 4, 5, 10, and 20 and total number of elements ranging from 24 to 120. We found that the solutions for $n = 3$, 5, 10 did not change with r_o/b ratios when the ratio is 5 or greater. Based on these studies we settled on a mesh with 40 elements and $r_o/b = 5$. The ring of elements surrounding the crack tip is formed with a singular plastic (9-noded) wedge element. This element choice and mesh design in conjunction with selective/reduced integration has been shown to give accurate solutions (Shih and Needleman, 1984a, 1984b).

Parameter Tracking. The solution to the nonlinear boundary value problem is obtained by the Newton-Raphson method. The iterative method is second order convergent if a close initial estimate of the solution is available. This initial estimate is generated by parameter tracking (Shih and Needleman, 1984a). Our numerical procedure begins by obtaining the solutions for $n = 3$, 5, 10 for a particular combination of displacements, say $R = 1$ and $\zeta = 0$. The solution for $n = 3$, $R = 1$ and $\zeta = 0$ is then employed as the initial estimate in the Newton-Raphson iterations for a slightly different value of ζ (the value of n and R are held fixed). A typical solution converges within 5 to 7 iterations. In this manner solutions for the complete range of displacement combinations are obtained with ζ serving as the tracking parameter. Solutions are obtained at ζ increments of 5 degrees; smaller increments are used in the range where the solutions change rapidly with respect to ζ as indicated in Tables 1 to 3.

Function Evaluations and Spline Fitting. Several quantities of interest can be evaluated directly from the field solutions which are obtained at distinct combinations of remotely applied displacements parameterized by ζ. In particular the total strain energy W is obtained by summing the element strain energy as defined by (2.5). Using (3.6), the values of f are then known at distinct values of ζ. To evaluate the derivative of f with respect to ζ the following approach is taken. We employ the natural cubic spline (Young and Gregory, 1972) to interpolate the distinct values of f and ζ. Values of f and f' at any value of ζ can then be determined directly from the spline functions (note that first and second derivatives of the spline interpolation function are continuous everywhere, Young and Gregory, 1972). Noting the periodicity of f (3.7) and of f', we have given values corresponding to ζ ranging from 0 to 180 deg. The values of the other functions listed in the tables are obtained by using the appropriate formulas given in Section 3 in conjunction with the tabulated values of f and f'.

Consistency Checks. We carried out several consistency checks. In one check, we calculated P and M using (3.8) and (3.9) and the tabulated values of f and f'. These values were found to be within 1 percent of the P's and M's calculated using (2.3) and the equivalent nodal forces associated with the nodes on the remote boundary Γ. We also evaluated the value of the J-integral using a volume integral (area integral in the case of two-dimensional problems) expression (Li et al., 1985) and the finite element field quantities evaluated at the 3 by 3 Gauss points. The J values associated with various (area) domains differed by less than 1 percent from the value determined from (3.11). For the constitutive relations considered in this paper (1.2) the surface of constant W (3.1) and Φ(3.2) must be convex in their respective displacement and force planes indicated in Fig. 2. A check of the values of f, f' and h, h' given in the tables showed that they satisfy the geometrical requirements associated with convexity. Finally, we add that the convergence of the rotation points (5.8) towards the Green and Hundy slip-line rotation point (1956) is an independent verification of the accuracy of the fully plastic solutions.